EPJ Web of Conferences **46**, 04004 (2013)
DOI: 10.1051/epjconf/20134604004

Angular Momentum Transport in Accretion Disk Boundary Layers Around Weakly Magnetized Stars

Martin E. Pessah[1,a] and Chi-kwan Chan[2,b]

[1] *Niels Bohr International Academy, Niels Bohr Institute, Blegdamsvej 17, 2100 Copenhagen Ø, Denmark*
[2] *NORDITA, Roslagstullsbacken 23, 106 91 Stockholm, Sweden*

Abstract. The standard model for turbulent shear viscosity in accretion disks is based on the assumption that angular momentum transport is opposite to the radial angular frequency gradient of the disk. This implies that the turbulent stress must be negative and thus transport angular momentum inwards, in the boundary layer where the accretion disk meets the surface of a weakly magnetized star. However, this behavior is not supported by numerical simulations of turbulent magnetohydrodynamic (MHD) accretion disks, which show that angular momentum transport driven by the magnetorotational instability (MRI) is inefficient in disk regions where, as expected in boundary layers, the angular frequency increases with radius. Motivated by the need of a deeper understanding of the behavior of an MHD fluid in a differentially rotating background that deviates from a Keplerian profile, we study the dynamics of MHD waves in configurations that are stable to the standard MRI. Employing the shearing-sheet framework, we show that transient amplification of shearing MHD waves can generate magnetic energy without leading to a substantial generation of hydromagnetic stresses. While these results are in agreement with numerical simulations, they emphasize the need to better understand the mechanism for angular momentum transport in the inner disk regions on more solid grounds.

1 Introduction

Most detailed calculations for determining the structure of the accretion disk boundary layer around a weakly magnetized star rely on effective models for turbulent angular momentum transport. These models are usually built as a turbulent version of the Newtonian viscous stress between fluid layers in a differentially rotating laminar flow [1], and thus assume a linear relationship between the stress and the angular frequency gradient, $d\Omega/dr$ [2]. This assumption, however, seems at odds with the properties of magnetohydrodynamic (MHD) turbulence revealed by numerical simulations of accretion disks [3–6] which show that angular momentum transport is inefficient in regions of the disk where $d\Omega/dr > 0$, which are stable to the standard magnetorotational instability (MRI) [7, 8]. In order to shed light into physically viable mechanisms for angular momentum transport in this inner disk region, we examine the generation of hydromagnetic stresses and energy density in differentially rotating backgrounds with angular frequencies that increase outward in the shearing-sheet framework.

[a] e-mail: mpessah@nbi.dk
[b] e-mail: ckch@nordita.org

2 Assumptions and Local Model for MHD Disk

We work in the framework of the shearing-sheet approximation [9, 10] and consider an ideal, weakly magnetized fluid characterized by an angular frequency $\boldsymbol{\Omega} = \Omega(r)\check{\boldsymbol{z}}$ and constant background density ρ_0. The local dynamics of this fluid is described by

$$\partial_t \boldsymbol{v} + (\boldsymbol{v}\cdot\nabla)\boldsymbol{v} = -2\Omega_0\check{\boldsymbol{z}}\times\boldsymbol{v} + 2q\Omega_0^2 x\check{\boldsymbol{x}} - \frac{\nabla P}{\rho_0} + \frac{(\boldsymbol{B}\cdot\nabla)\boldsymbol{B}}{4\pi\rho_0}\,, \tag{1}$$

$$\partial_t \boldsymbol{B} + (\boldsymbol{v}\cdot\nabla)\boldsymbol{B} = (\boldsymbol{B}\cdot\nabla)\boldsymbol{v}\,. \tag{2}$$

Here, $\boldsymbol{v}(\boldsymbol{x},t)$ and $\boldsymbol{B}(\boldsymbol{x},t)$, with $\nabla\cdot\boldsymbol{v} = \nabla\cdot\boldsymbol{B} = 0$, stand for the velocity and magnetic fields; and $\Omega_0 \equiv \Omega(r_0)$ is the angular frequency at a fiducial radius r_0. Because ρ_0 =const., we redefine the pressure and magnetic field so that $P/\rho_0 \to P$ and $\boldsymbol{B}/(4\pi\rho_0)^{1/2} \to \boldsymbol{B}$. We now decompose the flow into mean and fluctuations as $\boldsymbol{v}(\boldsymbol{x},t) \equiv \boldsymbol{U}_1(x) + \boldsymbol{u}(\boldsymbol{x},t)$ and $\boldsymbol{B}(\boldsymbol{x},t) \equiv \boldsymbol{B}_0(t) + \boldsymbol{b}(\boldsymbol{x},t)$, where $\boldsymbol{U}_1(x) \equiv -q\,\Omega_0 x\check{\boldsymbol{y}}$ and $\partial_t \boldsymbol{B}_0 = -q\,\Omega_0 B_{0x}\check{\boldsymbol{y}}$, and we have defined the shear parameter $q \equiv -(d\ln\Omega/d\ln r)_{r_0}$.

The substitution of these expressions into the previous set of equations leads to the following non-linear system for the dynamical evolution of the perturbations

$$\mathcal{D}_t\boldsymbol{u} - q\,\Omega_0 u_x\check{\boldsymbol{y}} = \boldsymbol{B}_0\cdot\nabla\boldsymbol{b} - 2\Omega_0\check{\boldsymbol{z}}\times\boldsymbol{u} - \nabla P, \tag{3}$$

$$\mathcal{D}_t\boldsymbol{b} + q\,\Omega_0 b_x\check{\boldsymbol{y}} = \boldsymbol{B}_0\cdot\nabla\boldsymbol{u}\,, \tag{4}$$

where the "semi-Lagrangian" time derivative $\mathcal{D}_t \equiv \partial_t + \boldsymbol{U}_1\cdot\nabla$ accounts for advection by the shearing background. Note that the equations above remain valid even if the amplitude of the perturbations is not small compared to the background values and they are exact as long as a single Fourier mode is considered [11]. Under these conditions, it is sensible to study the evolution of $\boldsymbol{u}(\boldsymbol{x},t)$ and $\boldsymbol{b}(\boldsymbol{x},t)$ for a long time.

In order to solve equations (3) and (4), it is convenient to work in Fourier space and use the ansatz $\boldsymbol{u}(\boldsymbol{x},t) = 2\mathrm{Re}\left[\hat{\boldsymbol{u}}_{\boldsymbol{k}'}(t)\exp(i\boldsymbol{k}'\cdot\boldsymbol{x}')\right]$ and $\boldsymbol{b}(\boldsymbol{x},t) = 2\mathrm{Re}\left[\hat{\boldsymbol{b}}_{\boldsymbol{k}'}(t)\exp(i\boldsymbol{k}'\cdot\boldsymbol{x}')\right]$, where the primes denote the shearing coordinate system $(x',y',z',t') \equiv (x, y+q\,\Omega_0 xt, z, t)$ in which $\mathcal{D}_t = \partial_{t'}$ [12], and $\boldsymbol{k}'\cdot\boldsymbol{x}' = \boldsymbol{k}(t)\cdot\boldsymbol{x} = (k'_x + q\,\Omega_0 tk'_y)x + k'_y y + k'_z z$. The equations for the Fourier amplitudes then become

$$d_t\hat{\boldsymbol{u}} - q\,\Omega_0\hat{u}_x\check{\boldsymbol{y}} = i\omega_{\mathrm{A}}\hat{\boldsymbol{b}} - 2\Omega_0\check{\boldsymbol{z}}\times\hat{\boldsymbol{u}} - i\boldsymbol{k}\hat{P}\,, \tag{5}$$

$$d_t\hat{\boldsymbol{b}} + q\,\Omega_0\hat{b}_x\check{\boldsymbol{y}} = i\omega_{\mathrm{A}}\hat{\boldsymbol{u}}\,. \tag{6}$$

Here, we have replaced $\partial_{t'}$ by d_t and omitted the subscripts $\boldsymbol{k}'$ in order to simplify the notation. We have also introduced the time-independent Alfvén frequency $\omega_{\mathrm{A}} \equiv \boldsymbol{B}_0(t)\cdot\boldsymbol{k}(t)$ [13].

3 Stress and Energy Density Associated with MHD-shearing Waves

The dynamical evolution of the modes with $\boldsymbol{k} \equiv k_z\check{\boldsymbol{z}}$ is quite simple; they grow exponentially if $k_z^2\omega_{\mathrm{A}}^2 \le 2q\Omega_0^2$ [14]. Thus, a Keplerian disk (with $q = 3/2$) can exhibit exponential growth but a shear profile with $q < 0$ only supports stable oscillations. In order to isolate the interesting dynamics that could arise from modes that are not associated with the MRI, we thus focus on modes with $k_z = 0$. By choosing the origin of time so that $k_x(t)$ is initially zero, we can use $k_x(t)$ to define our time coordinate so that $\tau \equiv k_x(t)/k_y \equiv q\,\Omega_0 t$. The divergence-less conditions then become $\tau\,\hat{u}_x + \hat{u}_y = \tau\,\hat{b}_x + \hat{b}_y = 0$, and thus the we only need to find $\hat{u}_x$ and $\hat{b}_x$ by solving the system

$$d_\tau\begin{pmatrix}\hat{u}_x\\ \hat{b}_x\end{pmatrix} = \begin{pmatrix}-\Gamma & i\omega\\ i\omega & 0\end{pmatrix}\begin{pmatrix}\hat{u}_x\\ \hat{b}_x\end{pmatrix}. \tag{7}$$

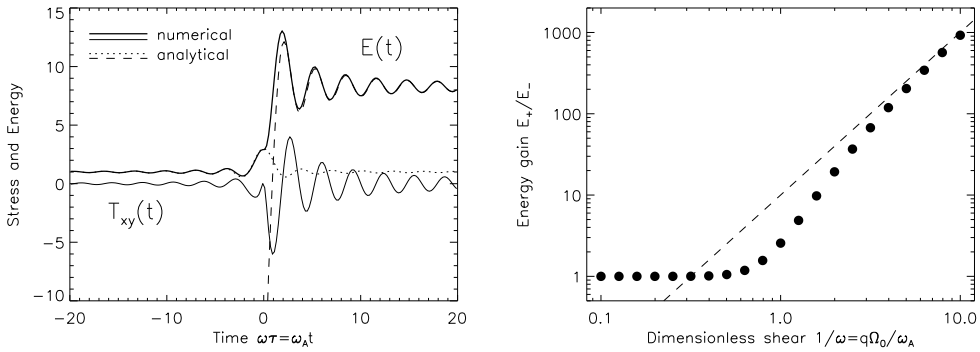

Figure 1. *Left*: The thick and thin solid lines correspond, respectively, to the total energy $E(t)$ and total stress $T_{xy}(t)$, calculated using the Fourier amplitudes $\hat{u}_x$, $\hat{u}_y$, $\hat{b}_x$, and $\hat{b}_y$ obtained numerically. The dotted and dashed lines show the analytical approximation for the energy. *Right*: The filled circles represent the value of the energy gain E_+/E_- for different values of the shear obtained via numerical integration using the initial conditions $C_- = 1$ and $S_- = 0$. In the limit of weak shear, there are only pure Alfvén waves and thus there is no net energy gain. The dashed line shows the function $10/\omega^2 \equiv 10(q\Omega_0/\omega_A)^2$, which is in good agreement with the numerical results for strong shear. This asymptotic behavior is independent of the initial conditions as long as $C_- \neq 0$.

It is worth mentioning that all the temporal dependence is contained in the factor $\Gamma(\tau) \equiv 2\tau/(\tau^2+1)$ and $\omega \equiv \omega_A/q\,\Omega_0$ is the dimensionless Alfvén frequency. The linear system (7) can be recast into one equation as $d_\tau^2\hat{b}_x + \Gamma(\tau)\,d_\tau\hat{b}_x + \omega^2\hat{b}_x = 0$, where the dependence on the parameters q, Ω_0, and ω_A is *only* through the combination $\omega^2 = (\omega_A/q\,\Omega_0)^2$. This equation does not have an analytical solution, but in the limit $\tau^2 \gg 1$, it reduces to a spherical Bessel equation, which possesses as solutions

$$\hat{u}_x = -\frac{C + S\,\omega\,\tau}{\omega^2\tau^2}\cos(\omega\,\tau) + \frac{S - C\omega\,\tau}{\omega^2\tau^2}\sin(\omega\,\tau), \tag{8}$$

$$\hat{b}_x = \frac{iC}{\omega\,\tau}\cos(\omega\,\tau) - \frac{iS}{\omega\,\tau}\sin(\omega\,\tau), \tag{9}$$

where S and C are complex constants determined by the initial conditions. Because these solutions are only valid for early/late times, we can approximate the (mean) total stress $T_{xy} \equiv \langle u_x u_y - b_x b_y\rangle$ and (mean) energy density $E \equiv \langle u^2 + b^2\rangle/2$ of the fluctuating fields [14] up to first order in $1/\omega\,\tau$ as

$$T_{xy} \approx -\frac{2}{\omega^2\tau}\Big[(|S|^2 - |C|^2)\cos(2\omega\,\tau) + (S^*C + S\,C^*)\sin(2\omega\,\tau)\Big], \tag{10}$$

$$E \approx -\frac{1}{\omega^3\tau}\Big[(|S|^2 - |C|^2)\sin(2\omega\,\tau) - (S^*C + S\,C^*)\cos(2\omega\,\tau)\Big] + \frac{1}{\omega^2}\left(|S|^2 - |C|^2\right) + |S'|^2 + |C'|^2\,, \tag{11}$$

where the asterisk denotes complex conjugation. Using these expressions, it is easy to see that the energy balance equation $d_t E = q\Omega_0 T_{xy}$ is also satisfied up to order $1/\omega\,\tau$.

In the left panel of Figure 1, we illustrate the numerical solutions for the stress $T_{xy}(t)$ and energy $E(t)$, given by the thin and thick solid lines, together with the analytical approximation for the energy. The latter has been obtained by substituting the two pairs of constants, $C_- = 1$ and $S_- = 0$, and $C_+ = 0.285$ and $S_+ = -1.896$, into equation (11). It is thus clear that the late-time stress oscillates around zero with decreasing amplitude, while the energy density asymptotes to a non-vanishing, time-independent value. The expression for the energy density at early/late times in terms of the constants

$S_\pm$ and $C_\pm$ is given by $E_\pm \equiv \lim_{t\to\pm\infty} E(t) = (|S_\pm|^2 + |C_\pm|^2)/\omega^2$. Therefore, the energy gain via swing amplification, E_+/E_-, is in general a function of the ratio $\omega = \omega_A/q\,\Omega_0$ and the initial conditions. We illustrate the dependence of the energy gain on the shear parameter in the right panel of Figure 1. In the limit of weak shear, there are only pure Alfvén waves and there is no net energy gain. The dashed line shows that the energy gain tends to the value $E_+/E_- = 10/\omega^2$ as $1/\omega \gg 1$, which provides a good description of the numerical results for strong shear. We have checked that the asymptotic behavior is insensitive to the initial conditions provided that the growing mode is excited, i.e. $C_- \neq 0$.

4 Discussion and Implications

We have seen that while the energy of the MHD waves can be significantly amplified, their net associated stresses oscillate around zero. This suggests that these shearing MHD waves are unlikely to play an important role in the transport of angular momentum in the accretion disk boundary layer region. These findings are consistent with the results of global MHD simulations of accretion disks with a rigid inner boundary carried out in [4] and [6]. These simulations show that the inner disk regions, where $d\Omega/dr \geq 0$, can develop strong toroidal magnetic fields, with associated magnetic energies that can easily reach a few tenths of the thermal energy, without leading to efficient angular momentum transport. The relationship between the stress and the radial gradient in angular frequency plays a key role when modeling the inner structure of the accretion disk surrounding a weekly magnetized star (see, e.g., [15–17]). Because of this, our results suggests that the detailed structure of these boundary layers could differ appreciably from the one derived within the standard framework of turbulent shear viscosity, where the direction of angular momentum transport is always opposite to the angular frequency gradient. The current availability of powerful numerical codes holds the promise that a more detailed understanding of MHD boundary layers will soon be possible (see [18] for a more detailed discussion of these and related issues).

References

[1] Landau, L. D., & Lifshitz, E. M. 1959, Fluid mechanics, ed. Landau, L. D. & Lifshitz, E. M.
[2] Lynden-Bell, D., & Pringle, J. E. 1974, MNRAS , 168, 603
[3] Abramowicz, M., Brandenburg, A., & Lasota, J.-P. 1996, MNRAS , 281, L21
[4] Armitage, P. J. 2002, MNRAS , 330, 895
[5] Pessah, M. E., Chan, C.-K., & Psaltis, D. 2008, MNRAS , 383, 683
[6] Steinacker, A., & Papaloizou, J. C. B. 2002, ApJ , 571, 413
[7] Balbus, S. A., & Hawley, J. F. 1991, ApJ , 376, 214
[8] Balbus, S. A., & Hawley, J. F. 1998, Reviews of Modern Physics, 70, 1
[9] Hill, G. 1878, Am. J. Math, Vol. 1, No. 2, pp. 129-147
[10] Goldreich, P., & Tremaine, S. 1978, ApJ , 222, 850
[11] Goodman, J., & Xu, G. 1994, ApJ , 432, 213
[12] Goldreich, P., & Lynden-Bell, D. 1965, MNRAS , 130, 125
[13] Balbus, S. A., & Hawley, J. F. 1992, ApJ , 400, 610
[14] Pessah, M. E., Chan, C.-K., & Psaltis, D. 2006, MNRAS , 372, 183
[15] Popham, R., & Narayan, R. 1991, ApJ , 370, 604
[16] Popham, R., Kenyon, S., Hartmann, L., & Narayan, R. 1996, ApJ , 473, 422
[17] Popham, R., & Narayan, R. 1995, ApJ , 442, 337
[18] Pessah, M. E., & Chan, C.-K. 2012, ApJ , 751, 48